Thermochimica Acta 496 (2009) 13–17

Contents lists available at ScienceDirect

Thermochimica Acta

journal homepage: www.elsevier.com/locate/tca

Thermal, solid–liquid equilibrium, crystallization, and microstructural studies of organic monotectic alloy: 4,4′-Dibromobiphenyl–succinonitrile

R.N. Rai*, R.S.B. Reddi

Department of Chemistry, Banaras Hindu University, Varanasi 221005, India

ARTICLE INFO

Article history:
Received 8 May 2009
Received in revised form 5 June 2009
Accepted 10 June 2009
Available online 18 June 2009

Keywords:
Phase diagram
Miscibility gap
Thermochemistry
Eutectic
Organic monotectic

ABSTRACT

The phase equilibrium data on an organic analogue of a metal–nonmetal system involving succinonitrile–4,4′-dibromobiphenyl shows two immiscible liquid phases are in equilibrium with a single liquid phase. The phase diagram study infers the formation of a eutectic and a monotectic with a large miscibility gap containing 0.9997 and 0.15 mole fractions of succinonitrile, respectively. The consolute temperature being 67.0 °C above the monotectic horizontal. The thermal study such as heat of mixing, entropy of fusion, roughness parameter, interfacial energy and excess thermodynamic functions were calculated from the enthalpy of fusion values, determined using differential scanning calorimeter (DSC) method. The effects of solid–liquid interfacial energy on morphological change of monotectic have also been discussed. The microstructures of monotectic, eutectic and pure components show their peculiar characteristic features.

1. Introduction

The investigations on the temperature dependent solidification behaviour of monotectic alloy are of potential importance both from fundamental understanding of the development of self-lubricating alloys and for industrial applications [1,2]. Although, metallic systems constitute an interesting area of investigations [3–5], they are not suitable for detail study due to high transformation temperature and wide density difference of the components involved. However, low transformation temperature, transparency, wider choice of materials and minimised convection effects are the special features that have prompted a number of research groups [6,7] to work on organic eutectics, monotectics and olecular complexes. As such organic systems are used as model systems for detailed investigation of the parameters which control the mechanism of solidification which decides the properties of materials. In addition, these materials are being used for various physicochemical investigations for their use for non-linear optical effects and different electronic applications [8–10].

The monotectic alloys have been less studied due to several difficulties associated with the miscibility gap systems while some of the articles [2,11,12] explain various interesting phenomena of monotectic alloys. The main problem arises due to a wide freezing range and large density difference between two liquid phases. The role of wetting behaviour, interfacial energy, thermal conductivity and buoyancy in a phase separation process has been the subject of great discussion. 4,4′-Dibromobiphenyl (DBBP) is a material of high enthalpy of fusion (28.38 kJ/mole) and simulates the nonmetallic solidification (faceted morphology) where as succinonitrile (SCN) is a material of low enthalpy of fusion (3.70 kJ/mole) and corresponds the metallic solidification (nonfaceted morphology). Therefore, the present DBBP–SCN system is very good organic analog of metal–nonmetal systems like Al–Si and Zn–Bi. In the present paper, the details concerning phase diagram, thermochemistry, linear velocity of crystallization at different undercoolings, heat of fusion, Jackson's roughness parameter, interfacial energy and microstructure of DBBP–SCN system are reported.

2. Experimental

2.1. Materials and purification

Succinonitrile, obtained from Aldrich, Germany, was purified by repeated distillation under reduced pressure while 4,4′-dibromobiphenyl (Aldrich, Germany) was used as received. The melting temperatures of DBBP and SCN were found to be 167.5 °C and 56.5 °C, respectively which are quite close to their respective values reported [13].

2.2. Phase diagram

The phase diagram of DBBP–SCN system was determined by the thaw–melt method in the form of temperature–composition curve. In this method [14,15], mixtures of two components covering the

* Corresponding author. Tel.: +91 0542 6701597; fax: +91 0542 2368127.
E-mail address: rn_rai@yahoo.co.in (R.N. Rai).

0040-6031/$ – see front matter © 2009 Published by Elsevier B.V.
doi:10.1016/j.tca.2009.06.012

entire range of compositions were prepared and these mixtures were homogenized by repeating the process of melting followed by chilling in ice cooled water 4–5 times. The melting points of completely miscible compositions and the miscibility temperatures of mixtures showing immiscibility were determined using a melting point apparatus (Toshniwal melting point) attached with a precision thermometer associated with an accuracy of ±0.5 °C.

2.3. Enthalpy of fusion

The values of heat of fusion of the pure components, the eutectic and the monotectic were determined [16,17] by differential scanning calorimeter (Mettelar DSC-4000 system). Indium sample was used to calibrate the system and the amount of test sample and heating rate were about 7 mg and 5 °C min^{-1}, respectively, for each estimation. The values of enthalpy of fusion are reproducible with in ±1.0%.

2.4. Growth kinetics

The growth kinetics of SCN–DBBP system was studied [15,16] by measuring the rate of movement of the solid–liquid interface at different undercoolings in a capillary tube of U-shape with about 150 mm horizontal portion and 5 mm internal diameter. Molten pure components, eutectic and monotectic were separately placed in a capillary in a thermostat containing silicone oil. The temperature of oil bath was maintained using microprocessor temperature controller of accuracy ±0.1 °C. At any desired temperature below the melting point of the sample, a seed crystal of the same composition was added to start nucleation, and the rate of movement of the solid–liquid interface was measured using a traveling microscope and a stop watch.

2.5. Microstructure

Microstructures of the pure components, the eutectic and the monotectic were recorded [14] by placing a drop of molten compound on a hot glass slide. To avoid the inclusion of the impurities from the atmosphere, a cover slip was glided over the melt and it was allowed to cool to get a super cooled liquid. The melt was nucleated with a seed crystal of the same composition at one end and care was taken to have unidirectional freezing. The slide with the unidirectional solidify sample was then placed on the platform of an optical (Leitz Labourlux D) microscope. Different regions were viewed and photographs of suitable magnification were taken with the help of camera attached with the microscope.

3. Results and discussions

3.1. Phase diagram

The phase diagram, between different compositions of DBBP–SCN and their melting/miscibility temperature, shows the formation of a monotectic and a eutectic as depicted in Fig. 1. The numerical values of different composition and its melting/miscibility temperature are tabulated in Table 1. Melting point of DBBP is 167.5 °C and it decreased by the addition of SCN. When the mole fraction of SCN is 0.15 immiscibility appears and at certain temperature the two liquids are completely miscible. With an increase in composition of SCN the miscibility temperature increases and it attains the maximum values when the mole fraction of SCN is 0.58. This maximum temperature also known as the upper consolute temperature (T_c) is 232.0 °C which is 67 °C above the monotectic horizontal (M_h). The both components are miscible in all proportions above the critical temperature. The thermal

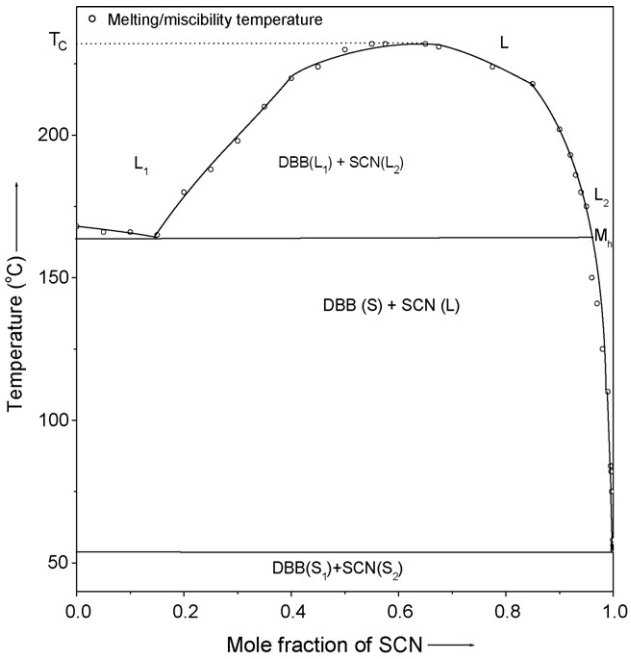

Fig. 1. Phase diagram of 4,4′-dibromobiphenyl–succinonitrile system (●) melting/miscibility temperature.

study of different compositions reveals that there are three reactions of interest, which occur isothermally on solidification. The first reaction concerns the phase separation in two liquids as the of single phase liquid, above 232.0 °C, is cooled below the critical

Table 1
Numerical values of solid–liquid equilibrium and liquid–liquid equilibrium temperature corresponding to different compositions.

Mole fraction of SCN	Melting/miscibility temperature
0.0000	167.5
0.0500	166.0
0.1000	166.0
0.1500	165.0
0.2000	180.0
0.2500	188.0
0.3000	198.0
0.3500	210.0
0.4000	220.0
0.4500	224.0
0.5000	230.0
0.5500	232.0
0.5750	232.0
0.6500	232.0
0.6750	231.0
0.7750	224.0
0.8500	218.0
0.9000	202.0
0.9200	193.0
0.9300	186.0
0.9400	180.0
0.9500	175.0
0.9600	150.0
0.9700	141.0
0.9800	125.0
0.9900	110.0
0.9950	84.0
0.9960	82.0
0.9970	75.0
0.9990	58.0
0.9996	56.0
0.9997	54.5
0.9999	55.5
1.0000	56.5

temperature (T_c), and can be written as

$$L \rightarrow L_1 + L_2$$

The direct observation on kinetics of phase separation from liquid L to $L_1 + L_2$ is interesting but the mechanism appears to be quite complicated. It seems that there is a disturbance in the whole liquid as a consequence of diffusion, collision between droplets, convection and movement by buoyancy driven fluid flow. A small decrease in temperature from the critical solution temperature is quite enough for the phase separation process to occur within few seconds. Although, in organic systems, the exact reason for the existence of miscibility gap is not clear, in the metallic systems the numbers of possibilities [18,19] such as compound formation tendencies, atomic radii difference, the valences differences of the component association, etc., or any of these might be responsible for the occurrence of the miscibility gap in the liquid state.

The second reaction, known as monotectic reaction, is quite similar to the eutectic reaction except that one of the product phases is a second liquid phase L_2 as follows:

$$L_1 \rightarrow S_1 + L_2$$

The third reaction is the eutectic reaction in which the liquid L_2 decomposes to give two solids as

$$L_2 \rightarrow S_1 + S_a$$

The monotectic, the eutectic and the critical solution temperatures in the present case are 165.0, 54.5 and 232.0 °C, respectively.

3.2. Growth kinetics

In order to study the crystallization behaviour of the pure components, the eutectics and the monotectics the crystallization rate (v) are determined at different undercoolings (ΔT) by measuring the rate of movement of solid–liquid interface in a capillary. The plots between $\log \Delta T$ and $\log v$ are given in Fig. 2 and the linear dependence of these plots are in accordance with the Hillig and Turnbull [20] equation:

$$v = u(\Delta T)^n \quad (1)$$

where u and n are constants depending on the solidification behaviour of the materials involved. The experimental values of these constants are given in Table 2. The value of u for the monotectic is being smaller than those of their pure components, and for the eutectic it is being in between the pure components. These results may be explained on the basis of the mechanism proposed by Winegard et al. [21]. According to this, in a binary system, eutectic/monotectic crystallization begins with the formation of the nucleus of one of the phases. The phase with metallic behaviour or with higher melting point one will start nucleating first. Since the phase with metallic behaviour solidifies with nonfaceted morphology and the enthalpy of fusion value is low and hence to start nucleation small amount of heat liberation would be required. This phase grows until the surrounding liquid becomes rich in the other component and a stage is reached when the second component also start nucleating. Now there are two possibilities, either the two initial crystals may grow side-by-side or there may be alternate nucleation of the two phases. It is evident from the Table 2 that the crystallization velocity of the monotectic is lower than the pure components and explains the alternate nucleation process of two phases involved. On the other hand, the rate of crystallization of the eutectic is in between the rate of crystallization of the pure components. The two phases of eutectic solidify and grow side-by-side mechanism. The difference in crystallization may be due to the difference in heat flow and the diffusion mode during monotectic and eutectic solidification.

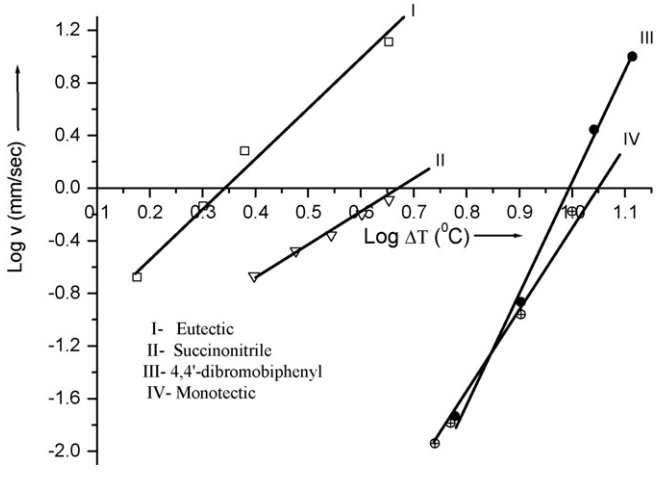

Fig. 2. Linear velocity of crystallization at various degrees of undercooling for 4,4′-dibromobiphenyl, succinonitrile and their eutectic and monotectic.

Table 2
Values of n and u for pure components, monotectic and eutectic.

Material	n	u (mm s^{-1}deg^{-1})
SCN	2.3	2.7×10^{-2}
DBBP	8.29	5.6×10^{-3}
Monotectic	6.7	1.1×10^{-6}
Eutectic	6.73	5.5×10^{-3}

4. Thermochemistry

4.1. Enthalpy of fusion

The values of enthalpy of fusion of the pure components, the eutectic and the monotectic, determined by the DSC method, are reported in Table 3. For comparison, the value of enthalpy of fusion of eutectic calculated by the mixture law [15] is also included in the same table. The enthalpy of mixing which is the difference of experimentally determined and the calculated values of the enthalpy of fusion are found to be 0.63 kJ mol^{-1}. As such, three types of structures are suggested [22]; quasi-eutectic for $\Delta_{mix}H > 0$, clustering of molecules for $\Delta_{mix}H < 0$ and molecular solution for $\Delta_{mix}H = 0$. The positive value of $\Delta_{mix}H$ for the eutectic suggests the formation of quasi-eutectic structure in the binary melt of the eutectic [23]. The entropy of fusion ($\Delta_{fus}S$) values, for different materials has been calculated by dividing the enthalpy of fusion by their corresponding absolute melting temperatures (Table 3). The positive values suggest that the entropy factor favours the melting process. The entropy of fusion value of eutectic is lower than that of the either of the components. This infers that the entropy factor is less effective in the melt of the eutectic and close to that of pure SCN [19].

Table 3
Heat of fusion, entropy of fusion and roughness parameter.

Materials	Heat of fusion (kJ mol^{-1})	Entropy of fusion (J mol^{-1} K^{-1})	Roughness parameter (α)
DBBP	28.38	64.4	7.8
SCN	3.70	11.2	1.4
DBBP–SCN monotectic (Exp.)	27.08	61.8	7.5
DBBP–SCN eutectic (Exp.) (Cal.)	3.08 3.71	9.4	1.1

Table 4
Critical radius of succinonitrile and 4,4′-dibromobiphenyl their eutectic and monotectic.

Undercooling ΔT (°C)	Critical radius $\times 10^{-8}$ (cm)			
	SCN	DBBP	Monotectic	Eutectic
1.5				13.25
2.0				9.94
2.4				8.28
2.5	6.8			
3.0	5.7			
3.5	4.9			
4.0	4.3			
4.5	3.8			4.42
5.5		2.32		
6.0		2.13	1.66	
8.0		1.59	1.25	
10.0		1.28		
11.0			0.91	
13.0			0.77	

Table 5
Interfacial energy of 4,4′-dibromobiphenyl, succinonitrile and their eutectic and monotectic.

Parameter	Interfacial energy (ergs cm^{-1})
σ_{SL_2} (SCN)	9.34
σ_{SL_1} (DBBP)	41.08
$\sigma_{L_1L_2}$ (DBBP–SCN)	11.25
σ_E (DBBP–SCN)	9.35

4.2. Size of critical nucleus and interfacial energy

When liquid is cooled below its melting temperature, it does not solidify spontaneously because, under equilibrium condition, the melt contains number of clusters of molecules of different sizes. As long as the clusters are well below the critical size [24], they cannot grow to form crystals and, therefore, no solid would result. The critical size (r^*) of nucleus is related to interfacial energy (σ) by the equation:

$$r^* = \frac{2\sigma T_{fus}}{\Delta_{fus}H\,\Delta T} \tag{2}$$

where T_{fus}, $\Delta_{fus}H$ and ΔT are melting temperature, heat of fusion, and degree of undercooling, respectively. An estimate of the interfacial energy is given by the expression:

$$\sigma = \frac{C\Delta_{fus}H}{(N_A)^{1/3}(V_m)^{2/3}} \tag{3}$$

where N_A is the Avogadro number, V_m is the molar volume, and parameter C lies between 0.30 and 0.35 [25]. The calculated values of critical nucleus at different undercoolings (the decrease in degree of temperature to that of melting point) and interfacial energy for different materials are reported in Tables 4 and 5, respectively.

4.3. Excess thermodynamic functions

The deviation from the ideal behaviour can best be expressed in terms of excess thermodynamic functions, namely, excess free energy (g^E), excess enthalpy (h^E), and excess entropy (s^E) which give a more quantitative idea about the nature of molecular interactions. The excess thermodynamic functions could be calculated [22,26] by using the following equations and the values are given in Table 6.

$$g^E = RT\left[x_1 \ln\ {\gamma_1}^l + x_2 \ln {\gamma_2}^l\right] \tag{4}$$

$$h^E = -RT^2\left[x_1\frac{\partial \ln\ {\gamma_1}^l}{\partial T} + x_2\frac{\partial \ln {\gamma_2}^l}{\partial T}\right] \tag{5}$$

$$s^E = -R\left[x_1 \ln {\gamma_1}^l + x_2 \ln {\gamma_2}^l + x_1 T\frac{\partial \ln {\gamma_1}^l}{\partial T} + x_2 T\frac{\partial \ln {\gamma_2}^l}{\partial T}\right] \tag{6}$$

where $\ln {\gamma_i}^l$, x_i and $\partial \ln {\gamma_i}^l/\partial T$ are activity coefficient in liquid state, the mole fraction and variation of log of activity coefficient in liquid state as function of temperature of a component i.

It is evident from Eqs. (4)–(6) that activity coefficient and its variation with temperature are required to calculate the excess functions. Activity coefficient (${\gamma_i}^l$) could be evaluated [15,22] by using the equation:

$$-\ln(x_i\gamma_i^l) = \frac{\Delta_{fus}H_i}{R}\left(\frac{1}{T_{fus}} - \frac{1}{T_i}\right) \tag{7}$$

where x_i, $\Delta_{fus}H_i$, T_i and T_{fus} are mole fraction, enthalpy of fusion, melting temperature of component i and eutectic melting temperature, respectively. The variation of activity coefficient with temperature could be calculated by differentiating Eq. (7) with respect to temperature

$$\frac{\partial \ln\ \gamma_i^l}{\partial T} = \frac{\Delta_{fus}H_i}{RT^2} - \frac{\partial x_i}{x_i \partial T} \tag{8}$$

$\partial x_i/\partial T$ in this expression can be evaluated by taking two points near the eutectic. The negative values of excess free energy indicate that there is an associative interaction between unlike molecules [26].

Table 6
Excess thermodynamic functions for the eutectic.

Material	g^E (kJ mol^{-1})	h^E (kJ mol^{-1})	s^E (J mol^{-1} K^{-1})
DBBP–SCN eutectic	−0.0172	−3.3523	−0.0102

4.4. Microstructure

It is well known that in polyphase materials the microstructure gives information about shape and size of the crystallites, which play a very significant role in deciding about mechanical, electrical, magnetic and optical properties of materials. The growth morphology [27,28] of a eutectic system is controlled by the growth characteristics of the constituent phases. According to Hunt and Jackson [29] the type of growth from melts depends upon the interface roughness (α) defined by

$$\alpha = \frac{\xi\Delta_{fus}H}{RT} \tag{9}$$

where ξ is a crystallographic factor which is generally equal to or less than one. The values of α are reported in Table 3. If $\alpha > 2$ the interface is quite smooth and the crystal develops with a faceted morphology. On the other hand, if $\alpha < 2$, the interface is rough and many sites are continuously available and the crystal develops with a non-faceted morphology.

4.4.1. The microstructure and growth of monotectic

In monotectic solidification when liquid of monotectic composition (Fig. 1) is allowed to cool, below the monotectic temperature (T_m), the stability of two liquid phases L_1, L_2 and a solid phase S at the solid–liquid interface are required. The necessary conditions for the stable three phases in contact have been explained by Chadwick [28]. Whether droplets nucleate in the melt or on the solid–liquid interface depends on the relative magnitude of the three interfacial energies. The requirement for the balance of interfacial energies gives the conditions:

$$\sigma_{SL_2} \leq \sigma_{SL_1} + \sigma_{L_1L_2} \tag{10}$$

and

$$\sigma_{SL_2} \geq \sigma_{SL_1} + \sigma_{L_1L_2} \tag{11}$$

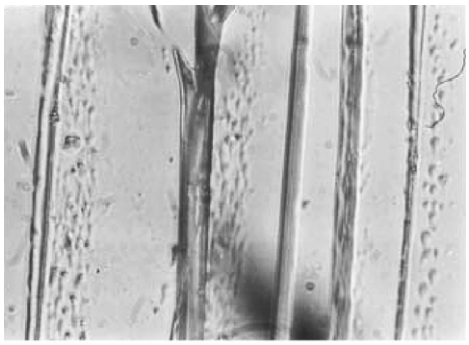

(a) Microstructure of monotectic X 220

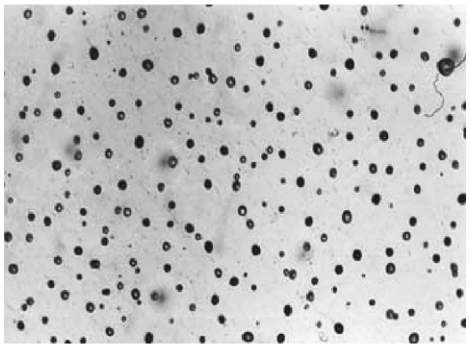

(b) Microstructure of eutectic X 220

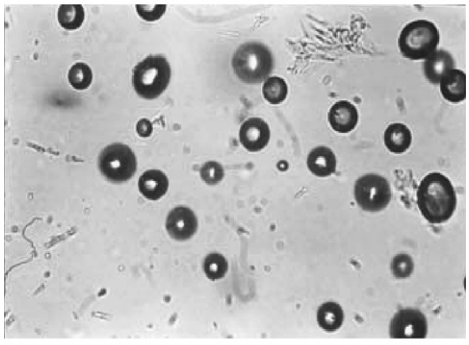

(c) Microstructure of eutectic X 260

Fig. 3. Directionally solidify optical microphotograph of 4,4′-dibromobiphenyl–succinonitrile monotectic (a) and (b) and (c) eutectic.

where σ_{SL_1}, σ_{SL_2} and $\sigma_{L_1L_2}$ are the interfacial energies of solid (S) and the liquid L_1, solid (S) and the liquid L_2, and liquids L_1 and liquid L_2, respectively. The surface energies were calculated by using the equation reported earlier [30], and has been tabulated in Table 5. The Cahn wetting condition [31] could be successfully applied to the present system as the interfacial energies are related by

$$\sigma_{SL_2} < \sigma_{SL_1} + \sigma_{L_1L_2}$$

Indicating that the DBB–SCN liquid (L_1) wets the solidified DBB perfectly. The directionally solidified optical microphotograph of monotectic Fig. 3(a) shows lamellar structure. The lamellar width and interspacing between lamella are not same. It is observed that where interspacing between lamella is large that is resulted the increase in lamellar width.

4.4.2. Microstructure of the eutectic

The view of eutectic microstructure indicates the perforate lamellar morphology Fig. 3(b). It seems lamellas have grown vertically and the microphotograph is the top view of the lamella. The magnified photograph of lamella (Fig. 3(c)) shows the circular shape which is diameter of lamellas.

5. Conclusions

The 4,4′-dibromobiphenyl–succinonitrile binary phase diagram was experimentally studied in detail which shows the formation of a monotectic and a eutectic with 0.15 and 0.9997 mole fractions of succinonitrile, respectively. The consolute temperature was found to be 67 °C above the monotectic horizontal. The growth behaviour of the pure components, the eutectic and the monotectic determined by measuring the rate of movement solid–liquid interface in a capillary suggest that growth data obey the Hillig–Turnbull equation. The entropy of fusion, enthalpy of mixing, excess thermodynamic functions and interfacial energy were calculated, using the values of enthalpy of fusion determined by the DSC method. The interfacial energies are related by the relation $\sigma_{SL_2} < \sigma_{SL_1} + \sigma_{L_1L_2}$ that confirms the applicability of Cahn wetting condition to the present system, while microstructural investigations shows lamellar growth morphology for monotectic and perforated lamellar growth morphology for the eutectic.

Acknowledgement

The authors would like to thank Board of Research in Nuclear Science, Department of Atomic Energy, Mumbai, India, for financial support.

References

[1] R.N. Grugel, A. Hellawel, Met. Trans. A 12 (A) (1981) 669–681.
[2] D.M. Herlach, R.F. Cochrane, I. Egry, H.J. Fecht, A.L. Greer, Int. Mater. Rev. 38 (1993) 273–347.
[3] R. Trivedi, W. Kurz, Int. Mater. Rev. 39 (2) (1994) 49–74.
[4] B. Majumdar, K. Chattopadhyay, Met. Trans. A 27 (A) (1996) 2053–2057.
[5] M.E. Glicksman, N.B. Singh, M. Chopra, Manuf. Space 11 (1983) 207–218.
[6] J. Teng, S. Liu, J. Cryst. Growth 290 (2006) 248–257.
[7] K. Pigon, A. Krajewska, Thermochim. Acta 58 (1982) 299–309.
[8] J.P. Farges, Organic Conductors, Marcel Dekker, Inc., New York, 1994.
[9] P. Gunter, Nonlinear Optical Effects and Materials, Springer-Verlag, Berlin, 2000, p. 540.
[10] N.B. Singh, T. Henningsen, R.H. Hopkins, R. Mazelsky, R.D. Hamacher, E.P. Supertzi, F.K. Hopkins, D.E. Zelmon, O.P. Singh, J. Cryst. Growth 128 (1993) 976–980.
[11] B. Derby, J.J. Favier, Acta Met. 7 (1983) 1123–1130.
[12] A. Ecker, D.O. Frazier, J.I.D. Alexander, Metall. Trans. 20A (1989) 2517–2527.
[13] H. Gilman, J. Org. Chem. 22 (1957) 447–449.
[14] R.N. Rai, J. Mater. Res. 99 (5) (2004) 1348–1355.
[15] U.S. Rai, R.N. Rai, Chem. Mater. 11 (11) (1999) 3031–3036.
[16] U.S. Rai, K.D. Mandal, Bull. Chem. Soc. Jpn. 63 (1990) 1496–1502.
[17] J.W. Dodd, K.H. Tonge, Thermal methods., in: B.R. Currel (Ed.), Analytical Chemistry by Open Learning, Wiley, New York, 1987, p. 120.
[18] B. Predel, J. Phase Equilib. 18 (4) (1997) 327–337.
[19] R.N. Rai, U.S. Rai, Thermochim. Acta 387 (2002) 101–107.
[20] W.B. Hillig, D. Turnbull, J. Chem. Phys. 24 (1956) 914.
[21] W.C. Winegard, S. Majka, B.M. Thall, B. Chalmers, Can. J. Chem. 29 (1951) 320–327.
[22] R.N. Rai, U.S. Rai, Thermochim. Acta 363 (2000) 23–28.
[23] U.S. Rai, R.N. Rai, J. Cryst. Growth 191 (1998) 234–242.
[24] J.W. Christian, The Theory of Phase Transformation in Metals and Alloys, Pergamon Press, Oxford, 1965, p. 992.
[25] D. Turnbull, J. Appl. Phys. 21 (1950) 1022–1028.
[26] N. Singh, B. Narsingh, U.S. Singh, O.P. Rai, Singh, Thermochim. Acta 95 (1985) 291–293.
[27] R. Elliot, Int. Metals Rev. 22 (1977) 161–186.
[28] G.A. Chadwick, Metallography of Phase Transformations, Butterworths, London, 1972, p. 312.
[29] J.D. Hunt, K.A. Jackson, Trans. Met. Soc. AIME 236 (1966) 843–852.
[30] U.S. Rai, R.N. Rai, J. Cryst. Growth 169 (1996) 563–569.
[31] J.W. Cahn, J. Chem. Phys. 66 (1977) 3667–3672.